Research Square

Preprints are preliminary reports that have not undergone peer review.
They should not be considered conclusive, used to inform clinical practice,
or referenced by the media as validated information.

Denoised gray matter BOLD-CSF coupling in aging and its association with markers of preclinical AD

Franziska Zistler

franziska.zistler@tum.de

Technical University of Munich

Julia Schwarz

Technical University of Munich

Leander Müller

Technical University of Munich

Gerhard Schneider

Technical University of Munich

Juliana Zimmermann

Technical University of Munich

Rachel Nuttall

Technical University of Munich

Article

Keywords: Gray matter BOLD-CSF coupling, aging, multi-echo fMRI, cerebrospinal fluid, fluid-crystallized ability discrepancy, cortical thickness

Posted Date: November 13th, 2026

DOI: https://doi.org/10.21203/rs.3.rs-11368503/v1

License: This work is licensed under a Creative Commons Attribution 4.0 International License.
Read Full License

Additional Declarations: No competing interests reported.

Title: Denoised gray matter BOLD-CSF coupling in aging and its association with markers of preclinical AD

Authors: Franziska Zistler[1]*, Julia Schwarz[1], Leander Müller[1], Gerhard Schneider[1], Juliana Zimmermann[1+], Rachel Nuttall[1+]

Affiliations:

[1] Technical University of Munich, School of Medicine and Health, Department of Anesthesiology and Intensive Care, Munich, Germany

* corresponding author

[+] shared last authorship

Corresponding author: Franziska Zistler, Email: franziska.zistler@tum.de

Word count: 2555

Figures: 4 (+1 Supplementary)

Tables: 3 (+1 Supplementary)

Abstract

Global gray matter (gGM) blood-oxygen-level-dependent (BOLD) signal fluctuations are temporally coupled with cerebrospinal fluid (CSF) inflow. Reduced gGM BOLD-CSF coupling has been reported in aging and linked to Alzheimer's disease (AD)-related pathology. Our study aimed to investigate the effect of multi-echo denoising on age-related reductions in coupling and whether coupling is associated with cortical thickness across AD-vulnerable regions and crystallized–fluid ability ('CF') discrepancy, markers of preclinical AD. We analyzed an open-access behavioral/MRI dataset (n=301) cognitively healthy younger and older adults (OpenNeuro ds003592). Coupling scores were calculated as correlations between gGM signal fluctuations and CSF inflow signals, before and after denoising. Linear mixed models tested the effects of age and denoising on coupling, while multiple regression models assessed associations between denoised coupling, cortical thickness, and CFdiscrepancy. Coupling was lower in older versus younger adults. Denoising significantly reduced coupling in younger adults but not in older adults. Both gGM and CSF signal amplitudes were lower in older adults. Denoised coupling was not significantly associated with cortical thickness or CFdiscrepancy, and cortical thickness was not associated with CFdiscrepancy after controlling for age. These findings support age-related differences in BOLD–CSF coupling, which itself may not be related to coarse markers of preclinical AD.

Keywords

Gray matter BOLD-CSF coupling, aging, multi-echo fMRI, cerebrospinal fluid, fluid-crystallized ability discrepancy, cortical thickness

Introduction

It has been hypothesized that clearance of waste products out of the brain, including amyloid-β and other solutes, is facilitated by a highly organized fluid transport system, called the glymphatic system [1]. In this model, there is a continuous circulation of cerebrospinal fluid (CSF flow) through and out of the parenchyma via the glymphatic pathway using the perivascular spaces created by the vascular endfeed of astrocytes. Subarachnoidal CSF enters the brain parenchyma along periarterial spaces flowing in the same direction as blood, mixes with interstitial fluid (ISF), and carries waste through perivenous spaces to meningeal and cervical lymph vessels [2].

CSF circulation depends on a tight coordination between all glymphatic components, including different cell types such as neurons, astrocytes, vascular and endothelial cells. Functional impairment in any of these components could lead to an impairment in fluid clearance. One important example are physiological changes associated with increasing age, such as arterial tortuosity, arterial stiffness due to high prevalence of arterial hypertension and abnormal resting vascular tone, among others (*see review* [3]). In mice, it has been shown that there is a decline in the efficiency of exchange between CSF and ISF in brain parenchyma in elderly specimens compared to young ones [4]. Reduced glymphatic function has been suggested to contribute to the progression of cognitive decline in aging, as well as the pathogenesis of Alzheimer's disease and possibly, to other neuropsychiatric diseases within the delirium spectrum [5]. Enhancement of this system could act as a potential therapeutic strategy to slow disease progression.

Functional resonance imaging (fMRI) studies in healthy adults looking at macroscopic CSF flow have found that brain-wide coactivity, e.g., global delta oscillations, can drive concordant vascular flow and volume effects, as measured by global blood oxygenation level-dependent (BOLD) signal, leading to strongly anticorrelated CSF inflow in the fourth ventricle (BOLD-CSF coupling) [6] and in the basal cisternae [7-11]. The statistical dependence, i.e., coupling, between fMRI global BOLD and CSF inflow signals reflects the interplay between (neurally-driven) vascular activity and macroscopic CSF flow. Cerebral CSF pulsations are driven by respiration, cardiac pulsations and neurally-driven slow vasomotor wave fluctuations, that in turn drive low frequency BOLD fluctuations [12]. Global gray matter (gGM) BOLD-CSF coupling hence serves as a proxy for the interplay between cerebral neural activity and CSF flow, reflecting the facilitation of CSF flow through neural activity [13].

Despite this well-described relationship, the link between ventricular CSF inflow and tissue, i.e., microscopic, glymphatic flux remains unclear. That being said, previous studies have found an association between weaker gGM BOLD-CSF coupling and neuropathological accumulation in Alzheimer's disease (AD) and Parkinson's disease [10,14,15], suggesting a relationship between this macroscopic metric of neurally-driven ventricular CSF inflow with glymphatic brain clearance. Interestingly, gGM BOLD-CSF coupling has been shown to be weaker in individuals who convert to the preclinical AD phase ([10,14,15]) - i.e. cognitively asymptomatic but with pathological accumulation in certain distributed cortical regions including medial and lateral temporal cortex, posterior lateral temporoparietal and medial parietal regions [16], suggesting that this coupling is sensitive to even the earliest stages of AD.

Despite positron emission tomography remaining the gold standard for measuring AD pathological accumulation [17], non-invasive correlates of AD pathological accumulation offer an alternative route for gaining insight into preclinical AD in asymptomatic subjects, when non-invasive techniques are preferred. Cognitive thinning in the regions described above has been associated with the accumulation of amyloid-β (Aβ) and hyperphosphorylated tau in the brain in preclinical AD, eventually leading to neurodegeneration [16,18-20]. Regional cognitive thickness can be estimated via cortical surface mapping of structural brain images acquired via magnetic resonance imaging. A cognitive-based metric has also been associated with pathological accumulation and cortical thinning in preclinical AD: the *discrepancy between crystallized and fluid abilities* ('FCdiscrepancy') [18]. Fluid abilities refer to performance in unfamiliar tasks involving complex problem-solving based on core cognitive domains such as working memory, reasoning and processing speed. Crystallized abilities, in contrast, refer to aspects of intelligence that draw on prior knowledge and experiences (e.g. vocabulary knowledge) [21]. Individuals with Alzheimer's disease (AD) exhibit a more rapid decline in fluid ability than in crystallized ability and the rate of decline in fluid ability has been associated with the progression of AD symptoms (e.g., [22-26]. In contrast, crystallized ability tends to remain relatively preserved during the early stages of AD [18]. In cognitively-healthy older-aged subjects, gGM BOLD-CSF coupling may also be related to cortical thinning and the FCdiscrepancy as non-invasive correlates of AD pathological accumulation.

Besides a relationship with neuropathological accumulation, gGM BOLD-CSF coupling has also been described to weaken with increasing age in healthy adults [15] more specifically starting at 55 years old and more strongly in females [11]. Several age-related structural and functional

alterations have been described, which could directly be mirrored in changed gGM BOLD signal, hence, impaired coupling. To name a few: reduced white matter integrity [27-29], reduced functional connectivity and network efficiency, particularly in higher-order cognitive networks [30,31], reduced regional efficiency of frontal, temporal hubs and limbic and paralimbic regions [32], less cognitive flexibility and additional recruitment of brain areas to perform tasks [33] and loss of volume, especially in prefrontal cortex (see review [34]). A recent publication has linked gGM BOLD-CSF coupling to resting-state 40-Hz gamma oscillations and suggested that coupling may influence the relationship between metabolic markers and cognitive performance in healthy aging [35].

Aside from physiological changes, artifacts such as increased motion in fMRI recordings in older-aged people compared with younger-aged people [36,37] have also been reported, which could significantly impact findings regarding age-related differences in gGM BOLD-CSF coupling. According to the equation $S(t) = S_0 e^{-t/T2^*}$, voxelwise fMRI signal intensity can be described by a monoexponential decay model. S(t) indicates the signal intensity measured at time *t* (S_0 therefore represents the signal intensity at t = 0 immediately following the radiofrequency excitation pulse). T2* corresponds to the effective transverse relaxation time constant, representing the rate of signal decay, where R2* = 1/T2*. Following radiofrequency excitation, the transverse magnetization gradually loses phase coherence as a result of spin–spin interactions and magnetic field inhomogeneities. This leads to an exponential decay of the measured MR signal over time, with higher R2* values reflecting a faster signal decay. The parameters S0 and R2* differ in their sensitivity to neuronal and non-neuronal sources of signal variation. Neuronal activity produces localized changes in cerebral blood oxygenation, generating the BOLD signal, which primarily affects R2* while having relatively little impact on S0. Conversely, non-neuronal sources of variability, such as head motion, scanner instabilities, respiration, and other artifacts, tend to influence S0 more strongly. Multi-echo imaging sequences capture multiple signals at different points along the signal decay curve following a single excitation. This allows BOLD-related signal changes to be distinguished from non-BOLD noise sources whose temporal or echo-dependent characteristics deviate from the expected signal decay profile [38]. Hence, multi-echo imaging allows non-BOLD noise sources to be removed from the data and offers an avenue along which one could establish the extent of which previously reported age-related reductions in gGM BOLD-

CSF coupling are attributable to higher motion tendencies and other noise sources in data from older adults.

This study used an open-access multi-echo resting-state fMRI dataset (OpenNeuro ds003592; Nathan Spreng; n = 301, 181 younger and 120 older adults) with an extensive cognitive battery to address four aims: (i) assess the effect of multi-echo denoising on age-related differences in gGM BOLD-CSF coupling; (ii) examine the predictive value of gGM BOLD-CSF coupling on the FCdiscrepancy; (iii) investigate the predictive value of gGM BOLD-CSF coupling on cortical thickness; and (iv) replicate the previously reported relationship between cortical thickness and the FCdiscrepancy.

Methods

Dataset

The data used in this study were derived from the publicly available repository OpenNeuro (accession number: ds003592) [39]. This included two 10-minute sessions of resting-state functional MRI (rs-fMRI) and an extensive battery of behavioural tests of 301 cognitively healthy volunteers within an age-range of 18 to 89 years old. Participants were classified in two groups, younger adults n=181 (mean age = 22.59 +/-3.27(s.d.)) and older adults n=120 (mean age = 68.63 +/- 6.44(s.d.)). Each participant completed the battery of cognitive, affective, and self-report measures prior to their scanning sessions [39]. For our purposes, the Dimensional Change Card Sort (nihcog_dccs), Flanker (nihcog_flanker), Picture Sequence Memory (nihcog_psm) and List Sorting Working Memory (nihcog_lswm) tests were used to calculate a composite fluid ability score and the Oral Reading Recognition Test (nihcog_orr) and Picture Vocabulary Test (nihcog_pva) tests were used to calculate a composite crystallized ability score per subject. These tests originate from the NIH Toolbox Cognition Battery developed as part of the NIH Blueprint for Neuroscience Research collaboration [40]. To address aims 1 and 3, 25 subjects were excluded, leaving 276 participants to be analyzed, with n=169 (mean age = 22.63 +/- 3.24(s.d.)) younger adults and n=107 (mean age = 68.34 +/- 6.37(s.d.)) older adults. To address Aims 2 and 4, a total of 224 participants were further excluded, leaving a sample size of 52 subjects. The reasons for exclusion of all excluded subjects can be found in Supplementary Table 1.

MRI acquisition and Preprocessing

Acquisition parameters. Imaging data were previously acquired at two sites, (i) with a 3 tesla GE Discovery MR750 and a 32-channel head coil at the Cornell Magnetic Resonance Imaging Facility in New York, USA, and (ii) with a 3T Siemens TimTrio MRI scanner and a 32-channel head coil at the New York University Neuroimaging Center in Toronto, Canada. *T1 anatomical image.* They used a T1 3D MPRAGE with the following parameters: site (i), time of repetition (TR) = 2530 ms, time to echo (TE) =3.4 ms, flip angle = 7°, voxel size = 1 mm isotropic with 2x acceleration with sensitivity encoding; site (ii), TR = 1900 ms, TE= 2.52 ms, flip angle = 9°, voxel size = 1 mm isotropic with 2x acceleration and generalized auto calibrating partially parallel acquisition (GRAPPA) encoding at an iPAT acceleration factor of 2. *BOLD functional images.* Two 10-minutes long eyes-open resting-state multi-echo gradient-echo echo-planar imaging (EPI) were used with the following scan

parameters: site (i), TR = 3000 ms; TE_1 = 13.7 ms, TE_2 = 30 ms, TE_3 = 47 ms; flip angle = 83°; matrix size = 72 × 72; field of view (FOV) = 210 mm; number of slices = 46; voxel size = 3 mm isotropic; volumes = 204, 2.5x acceleration with sensitivity encoding; site (ii), TR = 3000 ms; TE_1 = 14 ms, TE_2 = 29.96 ms, TE_3 = 45.92 ms; flip angle = 83°; matrix size = 64 × 64; FOV = 216 mm; number of slices = 43; voxel size = 3.4 × 3.4 × 3mm; volumes = 200, 3x acceleration and GRAPPA encoding.

Preprocessing of anatomical data. Anatomical data from each subject was processed using the Freesurfer 'recon-all', '@SUMA_Make_Spec_FS' and '@SSwarper' functions for volumetric segmentation, conversion to NIFTI format and skull stripping, respectively. From this pipeline, we derived a regional gray matter mask for each subject based on the Destrieux atlas [41], as well as regional estimates of cortical thickness based also on the Destrieux atlas.

Preprocessing of functional data. Multi-echo fMRI data were preprocessed using the afni_proc.py pipeline within AFNI [42,43]. The individual echo images were first preprocessed, including removal of the first four time points, slice-time correction (using windowed sinc interpolation using a 9-point window), volume registration to the volume in echo 2 automatically defined to contain the fewest outliers, and registration to the skull-stripped anatomical image. The preprocessed data from the individual echoes were then combined using a multi-echo independent component analysis approach implemented in *tedana v23.0.2* (https://github.com/ME-ICA/tedana) [44,45], which performs optimal combination of the echoes based on their echo-time (TE) dependence.

Motion correction. For each volume per session, the Euclidean norm of six realignment parameters (framewise displacement of 3 translation parameters and 3 rotation parameters) was calculated, and the maximum magnitude across all volumes was then obtained as an assessment of head motion. Subjects with a maximum Euclidean norm greater than 2.5 in at least one session were excluded from further analyses (n=7). For subsequent analyses, an additional scrubbing procedure was applied to minimize the influence of high-motion time points. Volumes with excessive motion (identified based on the Euclidean norm of the temporal derivatives of the six rigid-body motion parameters, using a threshold of 0.2) were excluded from the time series, together with the immediately preceding and following time points. If this resulted in at least 50% of the signal being removed, the respective scanning session was excluded from further analysis (n=15). The resulting motion-censored time courses were used for subsequent analyses.

Mask creation for time course extraction

Global gray matter BOLD (gGM BOLD) and CSF signals were extracted using individual, subject-specific masks (Figure 1). To generate the individual gGM masks, the skull-stripped T1-weighted anatomical image was registered to the denoised and optimally combined fMRI data from tedana. The resulting transformation was applied to the subject-specific gray matter mask obtained from Freesurfer. The transformed mask was binarized and subcortical regions were excluded, resulting in an individual whole-brain cortical gray matter mask. CSF masks were generated from the bottom slice from the volume-registered second-echo data (echo 2). The temporal standard deviation was calculated to identify regions with increased signal variability associated with CSF pulsatility. A spherical region of interest centered on the fourth ventricle was then applied to this image. An intensity threshold was used to exclude voxels containing no CSF signal, and the resulting image was binarized to generate an individual CSF mask. Mask generation was performed semi-manually, and all masks were visually inspected and manually corrected when necessary to ensure that only relevant CSF voxels were included.

Timecourses extraction and coupling approach

The mean gGM BOLD time series was extracted by applying the individual gGM masks to the denoised and optimally combined fMRI data. Due to extreme outlier values in the denoised gGM signal amplitude, two subjects were excluded from further analysis. To obtain CSF flow signal, the individual CSF masks were applied to the volume-registered second-echo data to obtain the mean CSF time series. Because the fMRI signal is sensitive to changes associated with CSF inflow, we focused on decreases in gGM BOLD activity. The first temporal derivative of the gGM BOLD time series was therefore calculated, and positive values were set to zero, retaining only periods of decreasing gGM BOLD signal. The first time point of the CSF time series was subsequently removed to account for the one-time-point reduction resulting from the derivative calculation. The temporal coupling between the resulting gGM and CSF time series was quantified using Pearson's correlation coefficient.

Calculation of the fluid-crystallized ability discrepancy score

The calculation of the FCdiscrepancy score was restricted to subjects with complete test results across all of the following tests: the Dimensional Change Card Sort (nihcog_dccs), Flanker

(nihcog_flanker), Picture Sequence Memory (nihcog_psm) and List Sorting Working Memory (nihcog_lswm) tests (used to calculate a composite fluid ability score) and the Oral Reading Recognition Test (nihcog_orr) and Picture Vocabulary Test (nihcog_pva) tests (used to calculate a composite crystallized ability score per subject) (n=26 subjects were incomplete and excluded). Participants younger than 60 years of age were excluded (n=147). To calculate the FCdiscrepancy score for each older-aged patient, the scores on each test were first z-transformed across subjects, following which a mean z-score was calculated across fluid and crystallized ability test groups as described above to create a composite fluid ability score and a composite crystallized ability score for each subject. Composite fluid ability score was subtracted from the composite crystallized ability score to create an FCdiscrepancy score per subject. Subjects with an FCdiscrepancy score less than 0 were excluded from further analysis as these subjects' scores might instead reflect non-dementia-related impairments [18]. A greater FCdiscrepancy score therefore indicated a relatively poorer performance in fluid ability tests than crystallised ability tests, a preclinical marker of AD.

Calculation of the cortical thickness composite score

Regional cortical thickness values were extracted from the Freesurfer pipeline as described previously. Specifically, values from the following regions within the Destrieux atlas were extracted for left and right hemisphere separately: inferior temporal gyrus, temporal pole, angular gyrus, superior frontal gyrus, superior parietal gyrus, supramarginal gyrus, precuneus, inferior frontal sulcus and the parahippocampal region (see Figure 2). These nine regions were chosen as they have been previously reported to be particularly vulnerable to AD neurodegeneration, showing cortical thinning even in asymptomatic Aβ-positive patients [16]. Left and right hemisphere values of average cortical thickness within each region were averaged together to form one estimate of cortical thickness within each of the nine regions-of-interest. Additionally, a mean cortical thickness value across all nine regions-of-interest was then calculated, creating a score of 'composite cortical thickness' within AD vulnerable regions per subject.

Further variables

Signal amplitudes. As previous studies have reported an association between gGM BOLD signal amplitude and gGM BOLD-CSF coupling [7,46], we additionally examined CSF and denoised gGM

signal amplitudes. For each participant, signal amplitude was calculated by subtracting the minimum value from the maximum value of each time series.

Statistics

Aim 1: *Assess the effect of the multi-echo denoising procedure on age-related differences in gGM BOLD-CSF coupling*

We aimed to investigate the effect of the multi-echo denoising procedure on the previously reported age-related reduction in gGM BOLD-CSF coupling. Normality was assessed using the Shapiro–Wilk test for each combination of group and noise condition. As Levene's tests showed that there was unequal variance between the age groups across both levels of the within-subject factor (denoised vs. non-denoised images), a linear mixed-effects model (LMM) was fitted using the nlme package in R [47], with group (older- vs younger-aged), noise condition (non-denoised vs denoised images), and their interaction as fixed effects, a participant-specific random intercept to account for repeated measurements, and a heterogeneous residual variance structure allowing residual variances to differ across the four group-by-noise combinations. The model was estimated using restricted maximum likelihood (REML). Furthermore, CSF and denoised gGM signal amplitudes were compared between younger and older adults using Mann-Whitney-U tests as data was non-normally distributed. Statistical significance of all statistical tests conducted was defined as $P < 0.05$ ($\alpha = 0.05$).

Aim 2: *Assess the predictive value of the gGM BOLD-CSF coupling on crystallized-fluid ability discrepancy*

To assess whether the FCdiscrepancy score can be predicted based upon the denoised gGM BOLD-CSF coupling value, we ran a linear regression model in R with the FCdiscrepancy score set as the outcome variable, the mean-centered denoised gGM BOLD-CSF coupling values as the predictor, with additional control variables: mean-centered age, sex, scanning site and (formula = FCdiscrepancy ~ (dn)gGM BOLD-CSF coupling + site + sex + age).

Aim 3: *Assess the predictive value of the gGM BOLD-CSF coupling on composite cortical thickness*

A linear regression model was estimated as above, but with the outcome set as the composite cortical thickness (formula = composite cortical thickness ~ (dn)gGM BOLD-CSF coupling + site + sex + age).

Aim 4: *Assess the relationship between composite cortical thickness and crystallized-fluid ability discrepancy*

With the goal of replicating previous findings, we conducted a partial correlation analysis to assess the relationship between composite cortical thickness and CFdiscrepancy across older-aged subjects after controlling for age. Partial correlation analysis via a Pearson's R test was conducted if data was found to be normally distributed, otherwise a Spearman's rank rho correlation test was conducted.

Results

Aim 1: *Assess the effect of the multi-echo denoising procedure on age-related differences in gGM BOLD-CSF coupling*

The tests of normality were all non-significant, suggesting normality in all conditions: coupling within the older-aged group based on non-denoised images (W= .985, P= .253) and denoised images (W= .978, P= .079), and within the younger-aged group based on non-denoised images (W= .996, P= .912) and denoised images (W= .994, P= .661). Preliminary Levene's tests indicated differences in coupling variability between the younger and older groups across the two noise conditions (non-denoised: $F(1, 274)= 4.21$, P= .041; denoised: $F(1, 274)= 6.51$, P= .011).

Our LMM results showed a significant main effect of age group, F(1,274)= 100.18, P<.001, indicating that coupling differed between younger and older participants. The main effect of noise condition was also significant, F(1,274)= 12.05, P<.001, indicating that the denoising procedure had a significant effect on coupling. The group-by-noise interaction was significant, F(1,275)= 9.77, P=.002, indicating that the effect of noise condition on coupling differed significantly between the two age groups (see Figure 3 and Table 1 for descriptive statistics).

Post-hoc pairwise comparisons based on estimated marginal means using the emmeans package in R revealed that coupling differed significantly between noise conditions in the younger group, with higher coupling based on the non-denoised images than the denoised images (mean difference= 0.023, SE= 0.005, t(274)= 4.657, P<.001). In contrast, no significant difference between noise conditions was observed in the older group (mean difference= -0.002, SE= 0.007, t(274)= -0.364, P= .716). However, upon inspection of the Q-Q plot of model residuals (Figure 4), there was

evidence of deviation from normality at the tails, suggesting that the residuals may not fully satisfy the normality assumption and may affect the reliability of statistical inference.

Our supplementary analyses on CSF and (denoised) GM signal amplitude differences between older and younger participants showed that GM signal amplitude was significantly lower in older adults (median= 50.920, IQR= 56.098) than in younger adults (median= 83.215, IQR= 59.599); Mann–Whitney U test (U= 4233.50, z= -7.441, P<.001) (Supplementary Figure 1). CSF signal amplitude was also significantly lower in older adults (median= 1544.02, IQR= 1476.06) than in younger adults (median= 1628.56, IQR= 437.294); Mann–Whitney U test (U= 7567, z= -2.282, P<.023) (Supplementary Figure 1).

Aim 2: *Assess the predictive value of the denoised gGM BOLD-CSF coupling on crystallized-fluid ability discrepancy*

The results of the linear regression model can be found in Table 2. The denoised gGM BOLD-CSF coupling was not significantly predictive of the CFdiscrepancy score in older-aged subjects after controlling for age, sex, education and site.

Aim 3: *Assess the predictive value of the gGM BOLD-CSF coupling on composite cortical thickness*

The results of the linear regression model can be found in Table 3. The denoised gGM BOLD-CSF coupling was not significantly predictive of the composite cortical thickness score after controlling for age, sex, education and site.

Aim 4: *Assess the relationship between composite cortical thickness and crystallized-fluid ability discrepancy*

The partial correlation analysis showed no significant correlation between composite cortical thickness and CFdiscrepancy after controlling for age (*rho*= -0.073, P= 0.613).

Discussion

In this study we investigated age-related differences in global gray-matter (gGM) BOLD-CSF coupling following a multi-echo-based denoising procedure and assessed whether individual differences in coupling is associated with crystallized-fluid ability discrepancy and cortical thickness, markers previously linked to preclinical Alzheimer's disease (AD) pathology. In line with previous studies, our results showed that gGM BOLD-CSF coupling was lower in older adults than in younger ones, regardless of whether the gray matter signal had been denoised or not. This suggests that previous findings of weaker gGM BOLD-CSF coupling with increasing age are robust against potential differences in noise contributions to fMRI across the lifespan. Complementarily, we also found that both gGM and CSF signal amplitudes were lower in older adults. Interestingly, the effect of denoising differed by age group: denoising significantly reduced coupling in younger adults, whereas no significant difference was observed in older adults. Whether this is a reflection of higher noise in our sample of fMRI data in the younger-aged group than the older-aged group could be one explanation, although this would be against our expectation and experience that older-aged subjects move more during scanning than younger-aged subjects. Due to the non-normality of our LMM residuals, this interaction effect could simply be a reflection of a poorly fit model. When inspecting raw data values, the difference in gGM BOLD-CSF coupling before and after denoising in the younger-aged group was not a particularly stark observation. Hence, we would suggest interpreting that finding with caution. Nonetheless, we believe our findings support the utility of the multi-echo approach in removing non-BOLD components from the fMRI data in order to estimate gGM BOLD-CSF coupling with higher accuracy.

Regarding the potential markers of preclinical AD, we did not find a significant relationship between gGM BOLD-CSF coupling and the crystallized-fluid ability discrepancy or composite cortical thickness after adjusting for covariates. One possible explanation for this could be that, especially due to our final sample size (n=52) for these analyses, within our relatively small pool of cognitively-healthy older-aged subjects, none or only a small number of subjects were in a preclinical AD stage. Without a significant number of asymptomatic subjects at the preclinical AD stage, the data wouldn't possess the variance needed to detect a relationship between the gGM BOLD-CSF coupling and markers of preclinical AD. This is potentially supported by the fact that we were also unable to replicate the previously reported finding of a significant association between composite cortical thickness and crystallized-fluid ability discrepancy after controlling for age [18].

However, previous studies based on Aβ imaging and autopsy results have shown that actually a range as high as 25-45% of cognitively-healthy older-aged subjects present Aβ burden [48-51], and gGM BOLD-CSF coupling has been shown to be sensitive to very early stages of Aβ burden in AD, even showing changes before the onset of accumulation ([10,14,15]). The crystallized-fluid ability discrepancy is an indirect cognitive marker, not a direct measure of Alzheimer's disease pathology and may be too coarse of a proxy metric to present an association with gGM BOLD-CSF coupling. Similarly, the absence of a significant association between denoised gGM BOLD-CSF coupling and composite cortical thickness does not rule out relationships with specific cortical regions. In particular, the superior frontal ROI used in the present study was relatively larger than the corresponding ROI in the original study from [18] and colleagues, which may limit direct comparability between findings.

This study has several limitations. To start with, the design of this investigation is cross-sectional, which means that our study cannot assess within-person changes over time. Furthermore, its retrospective nature is limited to the imaging, demographic, and cognitive variables available in the OpenNeuro ds003592 dataset. A prospective study would have been more appropriate. Second, it is important to highlight that our main measure, gGM BOLD-CSF coupling, reflects large-scale temporal coordination between BOLD and CSF signals and does not directly measure CSF circulation, glymphatic transport, or clearance efficiency; how this macroscopic coupling relates to the microscopic glymphatic pathway still needs to be clarified, therefore its interpretation as well. Third, despite the usage of multi-echo denoising, it is important to be aware that there might be further physiological factors still influencing the coupling of gGM and CSF, such as motion, and cardiorespiratory effects aliased in the signal and therefore influencing our results. Fourth, factors such as sleep and arousal states, hydration, caffeine intake, and underlying health conditions may contribute to interindividual variability of coupling and therefore the analysis. Overall, these findings highlight the importance of considering multi-echo denoising when studying gGM BOLD-CSF coupling, especially when looking into age related effects, and support further investigation of its potential relevance to preclinical AD in cognitively healthy adults.

Data availability statement: Data availability statement: The dataset analysed during the current study is publicly available from the OpenNeuro repository under accession number ds003592: https://openneuro.org/datasets/ds003592 [39]. No new datasets were generated during this study.

Reference list

1 Iliff, J. J. *et al.* A paravascular pathway facilitates CSF flow through the brain parenchyma and the clearance of interstitial solutes, including amyloid beta. *Sci Transl Med* **4**, 147ra111, doi:10.1126/scitranslmed.3003748 (2012).

2 Nedergaard, M. Neuroscience. Garbage truck of the brain. *Science* **340**, 1529-1530, doi:10.1126/science.1240514 (2013).

3 Jiang-Xie, L. F., Drieu, A. & Kipnis, J. Waste clearance shapes aging brain health. *Neuron* **113**, 71-81, doi:10.1016/j.neuron.2024.09.017 (2025).

4 Kress, B. T. *et al.* Impairment of paravascular clearance pathways in the aging brain. *Ann Neurol* **76**, 845-861, doi:10.1002/ana.24271 (2014).

5 Nedergaard, M. & Goldman, S. A. Glymphatic failure as a final common pathway to dementia. *Science* **370**, 50-56, doi:10.1126/science.abb8739 (2020).

6 Fultz, N. E. *et al.* Coupled electrophysiological, hemodynamic, and cerebrospinal fluid oscillations in human sleep. *Science* **366**, 628-631, doi:10.1126/science.aax5440 (2019).

7 Zimmermann, J. *et al.* Impaired Macroscopic Cerebrospinal Fluid Flow by Sevoflurane in Humans during and after Anesthesia. *Anesthesiology* **142**, 692-703, doi:10.1097/ALN.0000000000005360 (2025).

8 Berberich, C. *et al.* Increased coupling between global grey matter and CSF-derived fMRI signal in young adults after partial sleep deprivation - evidence from the sleepy brain study: Increased gGM-CSF-Coupling after sleep deprivation. *Neuroimage* **318**, 121420, doi:10.1016/j.neuroimage.2025.121420 (2025).

9 Zimmermann, J. *et al.* Total cerebral blood volume changes drive macroscopic cerebrospinal fluid flux in humans. *PLoS Biol* **23**, e3003138, doi:10.1371/journal.pbio.3003138 (2025).

10 Han, F. *et al.* Reduced coupling between cerebrospinal fluid flow and global brain activity is linked to Alzheimer disease-related pathology. *PLoS Biol* **19**, e3001233, doi:10.1371/journal.pbio.3001233 (2021).

11 Han, F., Liu, X., Yang, Y. & Liu, X. Sex-specific age-related differences in cerebrospinal fluid clearance assessed by resting-state functional magnetic resonance imaging. *Neuroimage* **302**, 120905, doi:10.1016/j.neuroimage.2024.120905 (2024).

12 Kiviniemi, V. *et al.* Ultra-fast magnetic resonance encephalography of physiological brain activity - Glymphatic pulsation mechanisms? *J Cereb Blood Flow Metab* **36**, 1033-1045, doi:10.1177/0271678X15622047 (2016).

13 Liu, X. Decoupling Between Brain Activity and Cerebrospinal Fluid Movement in Neurological Disorders. *J Magn Reson Imaging* **60**, 1743-1752, doi:10.1002/jmri.29148 (2024).

14 Tanaka, Y. *et al.* The coupling of global brain activity and cerebrospinal fluid flow as a potential predictive marker of brain amyloid-beta accumulation. *J Prev Alzheimers Dis* **12**, 100228, doi:10.1016/j.tjpad.2025.100228 (2025).

15 Han, F. *et al.* Decoupling of Global Brain Activity and Cerebrospinal Fluid Flow in Parkinson's Disease Cognitive Decline. *Mov Disord* **36**, 2066-2076, doi:10.1002/mds.28643 (2021).

16 Dickerson, B. C. *et al.* The cortical signature of Alzheimer's disease: regionally specific cortical thinning relates to symptom severity in very mild to mild AD dementia and is detectable in asymptomatic amyloid-positive individuals. *Cereb Cortex* **19**, 497-510, doi:10.1093/cercor/bhn113 (2009).
17 Rabinovici, G. D. *et al.* Updated appropriate use criteria for amyloid and tau PET: A report from the Alzheimer's Association and Society for Nuclear Medicine and Molecular Imaging Workgroup. *Alzheimers Dement* **21**, e14338, doi:10.1002/alz.14338 (2025).
18 McDonough, I. M. *et al.* Discrepancies between fluid and crystallized ability in healthy adults: a behavioral marker of preclinical Alzheimer's disease. *Neurobiol Aging* **46**, 68-75, doi:10.1016/j.neurobiolaging.2016.06.011 (2016).
19 Singh, V. *et al.* Spatial patterns of cortical thinning in mild cognitive impairment and Alzheimer's disease. *Brain* **129**, 2885-2893, doi:10.1093/brain/awl256 (2006).
20 Eskildsen, S. F. *et al.* Prediction of Alzheimer's disease in subjects with mild cognitive impairment from the ADNI cohort using patterns of cortical thinning. *Neuroimage* **65**, 511-521, doi:10.1016/j.neuroimage.2012.09.058 (2013).
21 Mungas, D. *et al.* Factor structure, convergent validity, and discriminant validity of the NIH Toolbox Cognitive Health Battery (NIHTB-CHB) in adults. *J Int Neuropsychol Soc* **20**, 579-587, doi:10.1017/S1355617714000307 (2014).
22 Albert, M. S. *et al.* The diagnosis of mild cognitive impairment due to Alzheimer's disease: recommendations from the National Institute on Aging-Alzheimer's Association workgroups on diagnostic guidelines for Alzheimer's disease. *Alzheimers Dement* **7**, 270-279, doi:10.1016/j.jalz.2011.03.008 (2011).
23 Bastin, C. & Salmon, E. Early neuropsychological detection of Alzheimer's disease. *Eur J Clin Nutr* **68**, 1192-1199, doi:10.1038/ejcn.2014.176 (2014).
24 McKhann, G. M. *et al.* The diagnosis of dementia due to Alzheimer's disease: recommendations from the National Institute on Aging-Alzheimer's Association workgroups on diagnostic guidelines for Alzheimer's disease. *Alzheimers Dement* **7**, 263-269, doi:10.1016/j.jalz.2011.03.005 (2011).
25 Schmid, N. S., Taylor, K. I., Foldi, N. S., Berres, M. & Monsch, A. U. Neuropsychological signs of Alzheimer's disease 8 years prior to diagnosis. *J Alzheimers Dis* **34**, 537-546, doi:10.3233/JAD-121234 (2013).
26 Tabert, M. H. *et al.* Neuropsychological prediction of conversion to Alzheimer disease in patients with mild cognitive impairment. *Arch Gen Psychiatry* **63**, 916-924, doi:10.1001/archpsyc.63.8.916 (2006).
27 Sullivan, E. V. & Pfefferbaum, A. Diffusion tensor imaging and aging. *Neurosci Biobehav Rev* **30**, 749-761, doi:10.1016/j.neubiorev.2006.06.002 (2006).
28 O'Sullivan, M. *et al.* Evidence for cortical "disconnection" as a mechanism of age-related cognitive decline. *Neurology* **57**, 632-638, doi:10.1212/wnl.57.4.632 (2001).
29 Pinto, M. S., Dos Santos, A. C. & Salmon, C. E. G. Age-related assessment of diffusion parameters in specific brain tracts correlated with cortical thinning. *Neurol Sci* **42**, 1799-1809, doi:10.1007/s10072-020-04688-9 (2021).
30 Geerligs, L., Renken, R. J., Saliasi, E., Maurits, N. M. & Lorist, M. M. A Brain-Wide Study of Age-Related Changes in Functional Connectivity. *Cereb Cortex* **25**, 1987-1999, doi:10.1093/cercor/bhu012 (2015).

31 Andrews-Hanna, J. R. *et al.* Disruption of large-scale brain systems in advanced aging. *Neuron* **56**, 924-935, doi:10.1016/j.neuron.2007.10.038 (2007).
32 Achard, S. & Bullmore, E. Efficiency and cost of economical brain functional networks. *PLoS Comput Biol* **3**, e17, doi:10.1371/journal.pcbi.0030017 (2007).
33 Chuikova, Z. *et al.* Aging-related changes in cognitive flexibility: fMRI meta-analysis. *Behav Brain Funct* **21**, 40, doi:10.1186/s12993-025-00301-1 (2025).
34 Hedden, T. & Gabrieli, J. D. Insights into the ageing mind: a view from cognitive neuroscience. *Nat Rev Neurosci* **5**, 87-96, doi:10.1038/nrn1323 (2004).
35 Lin, S. *et al.* Association of glymphatic function with 40-Hz neural oscillations, systemic metabolic markers, and cognitive performance in healthy aging adults: An EEG and MRI study. *Transl Psychiatry* **16**, doi:10.1038/s41398-026-04157-5 (2026).
36 Kato, S. *et al.* Effects of Head Motion on the Evaluation of Age-related Brain Network Changes Using Resting State Functional MRI. *Magn Reson Med Sci* **20**, 338-346, doi:10.2463/mrms.mp.2020-0081 (2021).
37 Van Dijk, K. R., Sabuncu, M. R. & Buckner, R. L. The influence of head motion on intrinsic functional connectivity MRI. *Neuroimage* **59**, 431-438, doi:10.1016/j.neuroimage.2011.07.044 (2012).
38 Power, J. D. *et al.* Ridding fMRI data of motion-related influences: Removal of signals with distinct spatial and physical bases in multiecho data. *Proc Natl Acad Sci U S A* **115**, E2105-E2114, doi:10.1073/pnas.1720985115 (2018).
39 Spreng, R. N. *et al.* Neurocognitive aging data release with behavioral, structural and multi-echo functional MRI measures. *Sci Data* **9**, 119, doi:10.1038/s41597-022-01231-7 (2022).
40 Baughman, R. W., Farkas, R., Guzman, M. & Huerta, M. F. The National Institutes of Health Blueprint for Neuroscience Research. *J Neurosci* **26**, 10329-10331, doi:10.1523/JNEUROSCI.3979-06.2006 (2006).
41 Destrieux, C., Fischl, B., Dale, A. & Halgren, E. Automatic parcellation of human cortical gyri and sulci using standard anatomical nomenclature. *Neuroimage* **53**, 1-15, doi:10.1016/j.neuroimage.2010.06.010 (2010).
42 Cox, R. W. AFNI: software for analysis and visualization of functional magnetic resonance neuroimages. *Comput Biomed Res* **29**, 162-173, doi:10.1006/cbmr.1996.0014 (1996).
43 Cox, R. W. & Hyde, J. S. Software tools for analysis and visualization of fMRI data. *NMR Biomed* **10**, 171-178, doi:10.1002/(sici)1099-1492(199706/08)10:4/5<171::aid-nbm453>3.0.co;2-l (1997).
44 Kundu, P., Inati, S. J., Evans, J. W., Luh, W. M. & Bandettini, P. A. Differentiating BOLD and non-BOLD signals in fMRI time series using multi-echo EPI. *Neuroimage* **60**, 1759-1770, doi:10.1016/j.neuroimage.2011.12.028 (2012).
45 Kundu, P. *et al.* Integrated strategy for improving functional connectivity mapping using multiecho fMRI. *Proc Natl Acad Sci U S A* **110**, 16187-16192, doi:10.1073/pnas.1301725110 (2013).
46 Muller, L. *et al.* Diurnal changes of cerebrospinal fluid and global signal coupling. *Neuroimage* **329**, 121833, doi:10.1016/j.neuroimage.2026.121833 (2026).
47 Pinheiro, J. B., D.; DebRoy, S.; Sarkar, D.; R Core Team. nlme: Linear and Nonlinear Mixed Effects Models. (2021).

48 Bennett, D. A. *et al.* Neuropathology of older persons without cognitive impairment from two community-based studies. *Neurology* **66**, 1837-1844, doi:10.1212/01.wnl.0000219668.47116.e6 (2006).
49 Mintun, M. A. *et al.* [11C]PIB in a nondemented population: potential antecedent marker of Alzheimer disease. *Neurology* **67**, 446-452, doi:10.1212/01.wnl.0000228230.26044.a4 (2006).
50 Pike, K. E. *et al.* Beta-amyloid imaging and memory in non-demented individuals: evidence for preclinical Alzheimer's disease. *Brain* **130**, 2837-2844, doi:10.1093/brain/awm238 (2007).
51 Price, J. L. & Morris, J. C. Tangles and plaques in nondemented aging and "preclinical" Alzheimer's disease. *Ann Neurol* **45**, 358-368, doi:10.1002/1531-8249(199903)45:3<358::aid-ana12>3.0.co;2-x (1999).

Author contributions: FZ and JS preprocessed and analyzed the data, RN and LM analyzed data, FZ and RN prepared figures, RN and JZ conceptualized the project, GS contributed to the research question and provided scientific and clinical supervision, FZ, JZ and RN wrote the main manuscript, all authors reviewed the manuscript.

Additional Information (including a Competing Interests Statement): The author(s) declare no competing interests.

Funding: This study was funded by institutional means (Department of Anesthesiology and Intensive Care from the Technical University of Munich (TUM) University Hospital). The authors received no external funding for this work.

Figure legends

Figure 1. Exemplary masks from a representative subject. Global gray matter BOLD (gGM BOLD, a, red) and CSF signals (b, blue) in the foramen magnum are shown overlaid on the corresponding axial fMRI slice. These masks were subsequently used to extract gGM and CSF signals from the resting-state fMRI data. Below (c), example time courses of gGM (red) and CSF signals (blue) are visualized as percent signal change scores in a representative subject.

Figure 2. Regions-of-interest for calculating the composite cortical thickness score per subject. Brain surface renderings display the nine cortical regions-of-interest shown in distinct colors, across multiple views. These regions are reportedly vulnerable to Alzheimer's disease-related pathology at preclinical stages. Gray areas indicate regions not highlighted in the current map (NA). Composite cortical thickness was calculated as the average cortical thickness across all nine regions.

Figure 3. Gray matter BOLD–CSF coupling in younger- and older-aged groups before and after denoising. Violin plots show the distributions of gray matter BOLD–CSF coupling coefficients (r) for younger-aged (yellow) and older-aged (turquoise) participants using denoised and non-denoised gray matter signal. Embedded boxplots indicate the median and interquartile range, with whiskers representing the spread of the data.

Figure 4. Normal Q–Q plot of normalized residuals from the linear mixed-effects model. The quantiles of the model's normalized residuals are plotted against the theoretical quantiles of a normal distribution to assess the normality assumption. The red reference line indicates the expected relationship under normality; the deviations from this line at the tails suggest the presence of potential outliers that deviate from a normal residual distribution.

Tables

Age group	Image noise	n	mean	SD
older	non-denoised	107	0.161	0.126
older	denoised	107	0.164	0.11
younger	non-denoised	169	0.339	0.149
younger	denoised	169	0.315	0.143

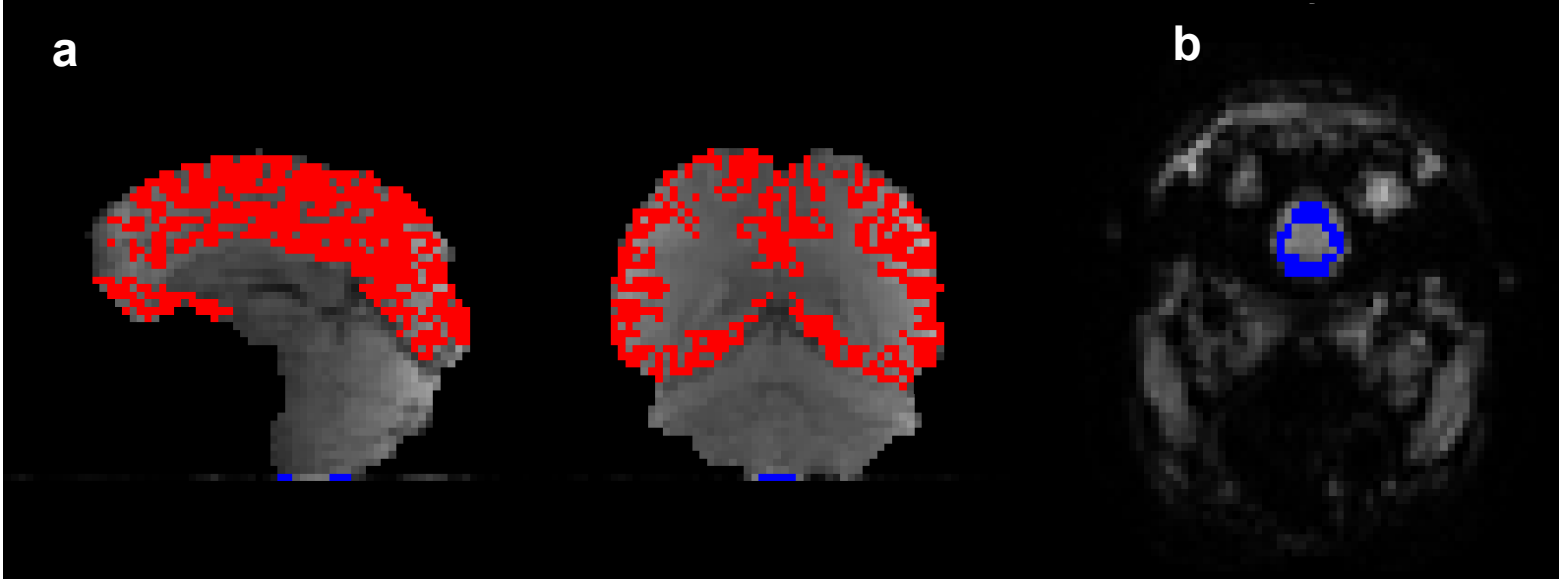
Table 1. Descriptive statistics of the gGM BOLD-CSF coupling across age group and noise conditions.

Predictor	**Crystallized-fluid ability discrepancy**			
	β	*SE*	*t*	*P*
Intercept	0.438	0.399	1.097	0.278
Denoised gGM BOLD-CSF coupling	0.432	0.762	0.567	0.573
Site	**-0.425**	**0.189**	**-2.252**	**0.029**
Sex	-0.134	0.149	-0.897	0.374
Age	**0.034**	**0.013**	**2.674**	**0.010**
Res. SE	**0.518**			
R^2	**0.205**			
Adj. R^2	**0.137**			
F	**3.03**			
P	**0.027**			

Table 2. Results of the multiple linear regression model predicting crystallized-fluid ability discrepancy based on denoised gGM BOLD-CSF coupling, controlling for site, sex and age. The entries in bold indicate significant results with P<0.05.

Predictor	**Composite cortical thickness**			
	β	*SE*	*t*	*P*
Intercept	**2.601**	**0.063**	**41.541**	**<.001**
Denoised gGM BOLD-CSF coupling	-0.149	0.119	-1.246	0.219
Site	**0.104**	**0.030**	**3.533**	**<.001**
Sex	0.009	0.023	0.380	0.706
Age	**-0.005**	**0.002**	**-2.429**	**0.019**
Res. SE	**0.081**			
R^2	**0.288**			
Adj. R^2	**0.227**			
F	**4.752**			
P	**0.003**			

Table 3. Results of the multiple linear regression model predicting composite cortical thickness based on denoised gGM BOLD-CSF coupling, controlling for site, sex and age. The entries in bold indicate significant results with P<0.05.



c

PSC of gGM-BOLD (%)

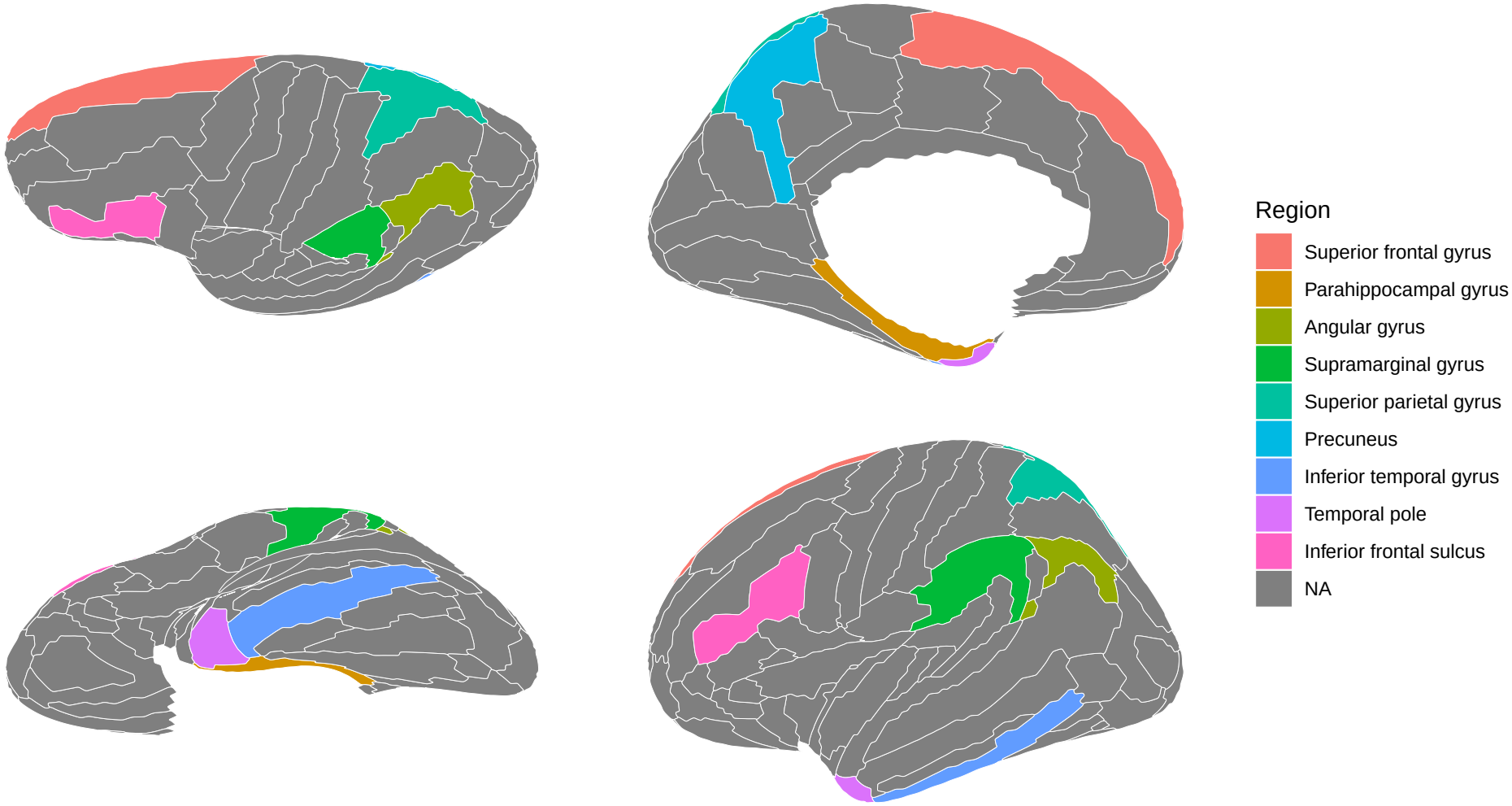
PSC of CSF (%)

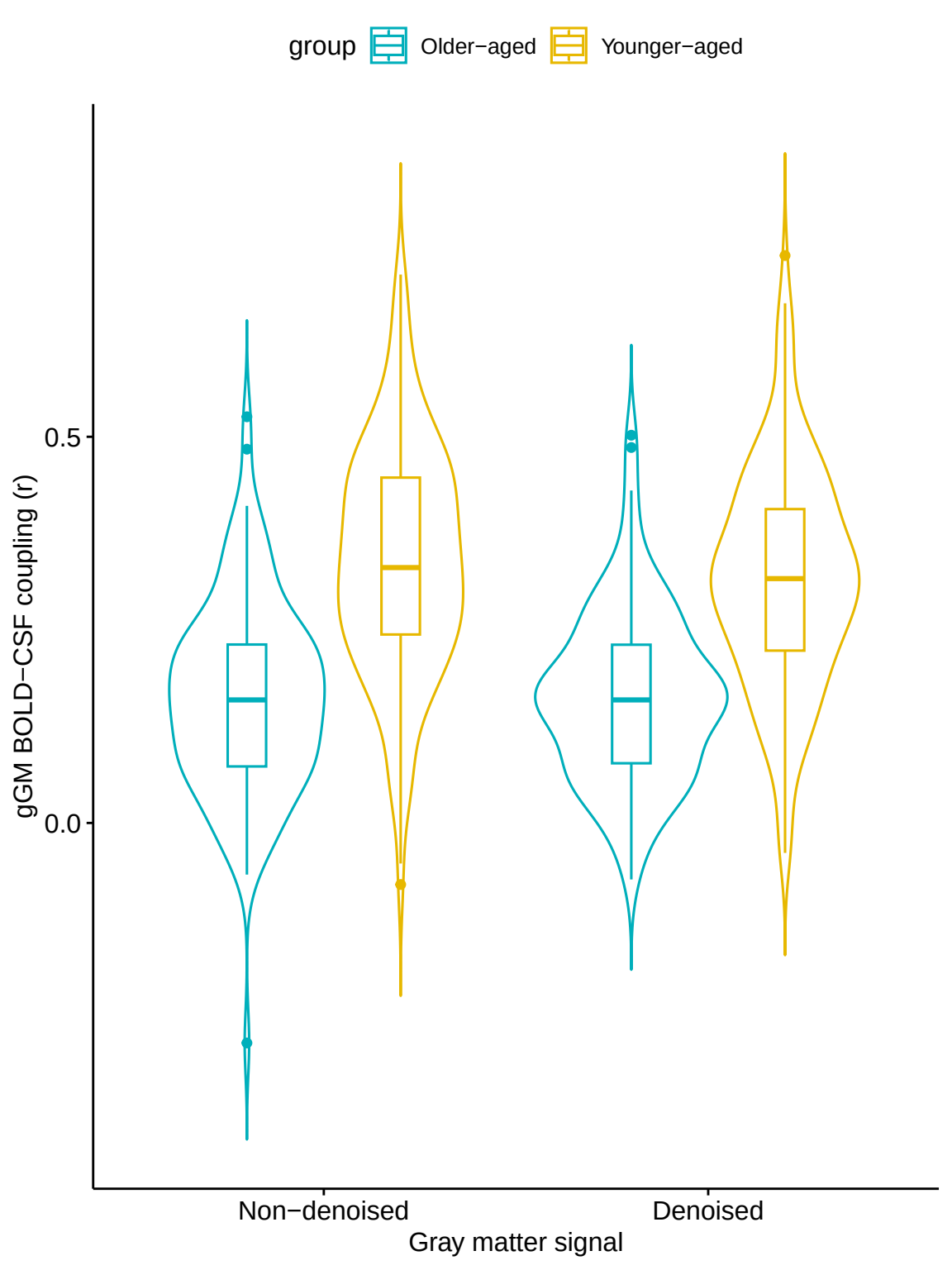
Timepoints

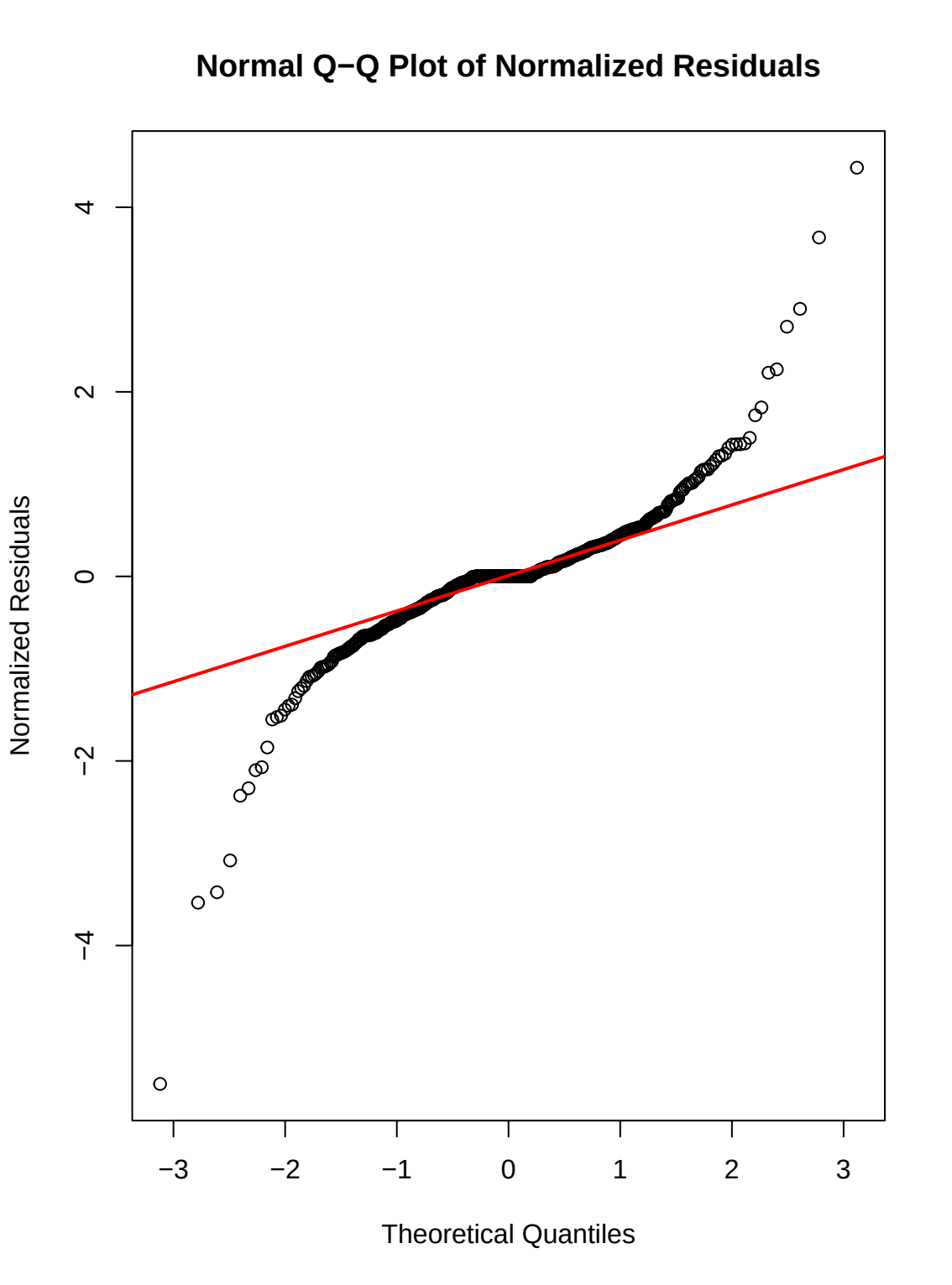
gGM

gGM denoised

CSF


Region
Superior frontal gyrus
Parahippocampal gyrus
Angular gyrus
Supramarginal gyrus
Superior parietal gyrus
Precuneus
Inferior temporal gyrus
Temporal pole
Inferior frontal sulcus
NA


group
Older−aged
Younger−aged
0.5
0.0
gGM BOLD−CSF coupling (r)
Non−denoised
Denoised
Gray matter signal


Normal Q−Q Plot of Normalized Residuals
Normalized Residuals
Theoretical Quantiles
4
2
0
−2
−4
−3
−2
−1
0
1
2
3

Supplementary Files

This is a list of supplementary files associated with this preprint. Click to download.

- DenoisedCouplingAgeingSupplement.docx